

Gaps in globular cluster streams: giant molecular clouds can cause them too

Nicola C. Amorisco^{1,2*}, Facundo A. Gómez², Simona Vegetti², Simon D.M. White²

¹*Institute for Theory and Computation, Harvard-Smithsonian Center for Astrophysics, 60 Garden St., MS-51, Cambridge, MA 02138, USA*

²*Max Planck Institute for Astrophysics, Karl-Schwarzschild-Strasse 1, D-85740 Garching, Germany*

8 June 2022

ABSTRACT

As a result of their internal dynamical coherence, thin stellar streams formed by disrupting globular clusters (GCs) can act as detectors of dark matter (DM) substructure in the Galactic halo. Perturbations induced by close flybys amplify into detectable density gaps, providing a probe both of the abundance and of the masses of DM subhaloes. Here, we use N-body simulations to show that the Galactic population of giant molecular clouds (GMCs) can also produce gaps (and clumps) in GC streams, and so may confuse the detection of DM subhaloes. We explore the cases of streams analogous to the observed Palomar 5 and GD1 systems, quantifying the expected incidence of structure caused by GMC perturbations. Deep observations should detect such disturbances regardless of the substructure content of the Milky Way’s halo. Detailed modelling will be needed to demonstrate that any detected gaps or clumps were produced by DM subhaloes rather than by molecular clouds.

Key words: galaxies: haloes — cosmology: theory — dark matter — galaxies: kinematics and dynamics — galaxies: structure

1 INTRODUCTION

The ability to reproduce large-scale cosmological observations is a great success of the standard Λ CDM structure formation model (e.g., Planck Collaboration 2014; Gott et al. 2005; Anderson et al. 2014) but is independent of the nature of the dark matter. Various dark matter models share this success, but make different predictions for the amount and properties of structure on scales of galaxy haloes and smaller. Standard WIMP/axion CDM predicts galaxy haloes that host a multitude of bound subhaloes, the remnants of earlier halo generations (DSs, e.g., Moore et al. 1999; Klypin et al. 1999; Gao et al. 2004; Diemand et al. 2008; Springel 2008). Such a population is substantially suppressed in warm DM models as a result of a cut-off in the linear power spectrum at small mass scales ($M \lesssim 10^8 M_\odot$, e.g., Colín et al. 2000; Bode et al. 2001; Menci et al. 2012; Macciò et al. 2013), while self-interacting DM models also predict both a reduction in the DS population and variations in their internal structural properties (e.g., Vogelsberger et al. 2012; Rocha et al. 2013). The characterisation of low mass DSs thus represents a promising route to advance our understanding of DM.

Great interest has been sparked by the realisation that thin globular cluster (GC) streams in the Milky Way (MW)

could reveal the presence of DSs, by showing distinctive signs of flyby encounters (Ibata et al. 2002; Johnston et al. 2002). The internal dynamics of kinematically cold streams are such that perturbations induced by a gravitational encounter are amplified with time: coherent shifts in the energy distribution of stream stars near closest approach result in the formation of under-dense regions, usually referred to as gaps (e.g., Yoon et al. 2011; Carlberg 2013; Erkal & Belokurov 2015; Sanders et al. 2016) as well as over-dense clumps and even kinks (e.g. Ngan & Carlberg 2014; Ngan et al. 2016). This makes GC streams with internal velocity dispersions of a few km/s potentially sensitive to encounters of DSs with masses as small as $M \sim 10^5 M_\odot$. The detection of a population of such DSs would put stringent constraints on the nature of DM.

Two spectacular examples of thin GC streams are those of Palomar 5 (Pal5, Odenkirchen et al. 2002, 2003; Grillmair & Dionatos 2006a) and GD1 (Grillmair & Dionatos 2006b), for both of which the density profile can be mapped over ~ 10 kpc in length using SDSS data (e.g., Carlberg 2012; Koposov et al. 2010). Interestingly, both streams display substructure with amplitude that appears marginally higher than expected due to observational (counting) noise alone (Carlberg 2012, 2016), suggesting the possibility that external perturbations are indeed important.

In this Letter, we show that the Galactic population of giant molecular clouds (GMCs) is expected to produce gaps

* E-mail: nicola.amorisco@cfa.harvard.edu

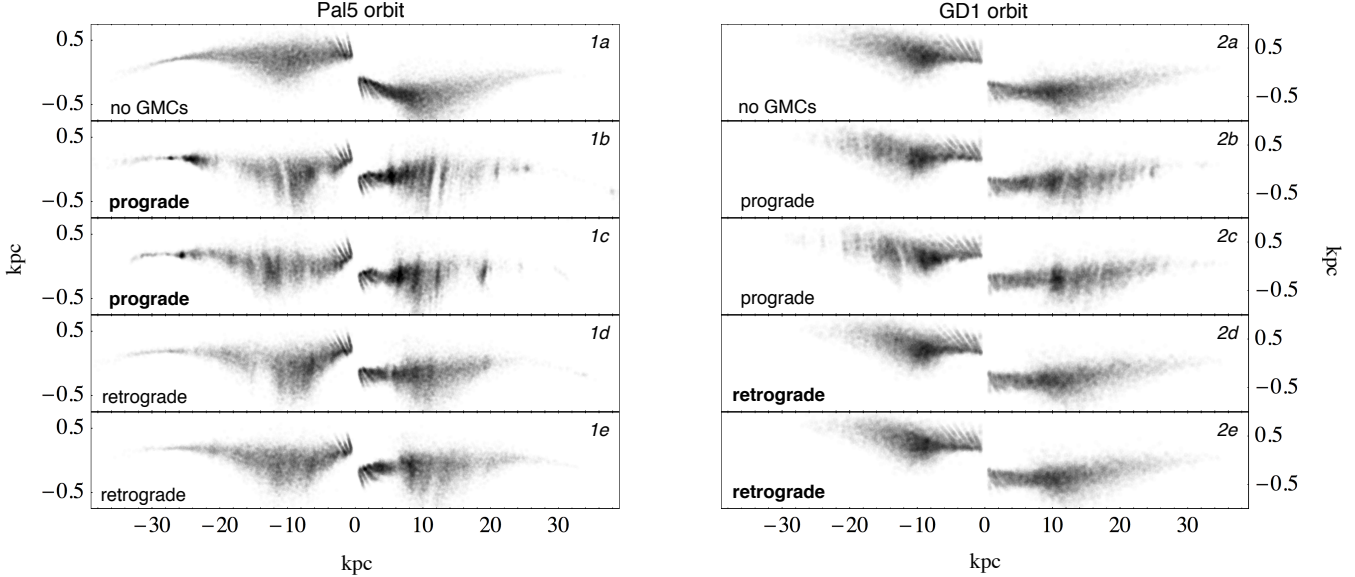


Figure 1. Examples of GC streams on Pal5- and GD1-like orbits, straightened along the remnant’s trajectory. Panels *1a* and *2a* show unperturbed streams. All other panels show the stream when a disk of giant molecular clouds is added. Panels *1b-c* and *2b-c* show streams on prograde orbits. Panels *1d-e* and *2d-e* show the corresponding retrograde streams, where the increased relative velocity of close encounters reduces perturbation amplitudes.

and clumps in the Pal5 and GD1 streams which are similar to those that would be induced by DSs, thus significantly complicating the detection of halo substructure. We explore this process using N-body simulations of stream formation in the presence of a disk of GMCs, but ignoring any DM substructure. We quantify the abundance and properties of the gaps and clumps produced, thus characterising the confusing background against which the effects of DSs must be identified.

2 N-BODY SIMULATIONS

We use Gadget2 (Springel 2005) to compute the evolution of GC streams with orbits similar to Pal5 and GD1 within a three-component, static approximation to the MW’s potential taken from Errani et al. (2015). In all runs, the progenitor GC is represented by a self-gravitating, isotropic Plummer sphere with a mass of $10^{4.8} M_{\odot}$, a half-mass radius of $r_h = 16$ pc, and 10^5 equal-mass “stars”. In agreement with the inferred orbital properties (e.g. Odenkirchen et al. 2002; Grillmair & Dionatos 2006a; Küpper et al. 2015; Fritz & Kallivayalil 2015), our Pal5-like runs have $(r_{\text{per}}, r_{\text{apo}}, i) = (8 \text{ kpc}, 19 \text{ kpc}, 65^{\circ})$, where r_{per} , r_{apo} and i are respectively pericentric radius, apocentric radius and inclination with respect to the stellar disk. This results in an orbital period $T_r = 0.30$ Gyr. Our GD1-like runs have $(r_{\text{per}}, r_{\text{apo}}, i) = (12 \text{ kpc}, 27 \text{ kpc}, 35^{\circ})$ (e.g. Grillmair & Dionatos 2006b; Willett et al. 2009; Koposov et al. 2010; Bowden et al. 2015) for a period of $T_r = 0.44$ Gyr. All runs start with the GC at its orbital apocenter, and follow it for 10 Gyr. While Pal5 and GD1 are observed to be prograde and retrograde, respectively, with respect to the sense of rotation of the stellar disk, we explore both prograde and retrograde configurations for both orbits.

Our GMC populations have a total mass of $M_{\text{tot}} =$

$10^9 M_{\odot}$, 69% of which lie between a radius of 2 kpc and the solar radius, $R_{\odot} = 8.5$ kpc, the remainder is at larger radii. GMCs are confined to a razor-thin disk that, at R_{\odot} , breaks from an inner scale-length of 2.5 kpc to an outer one of 3.9 kpc (Heyer & Dame 2015). We generate individual GMC masses by adopting the results of Rice et al. (2016), which report a steep GMC mass function outside R_{\odot} (an average power-law slope of $\alpha \sim -2.2$ for masses $M_{\text{GMC}} > 10^5 M_{\odot}$, where $dN/dM_{\text{GMC}} \propto M_{\text{GMC}}^{-\alpha}$). The mass function within R_{\odot} is less steep ($\alpha \sim -1.5$), although it truncates sharply with no GMCs at $M_{\text{GMC}} \geq 10^7 M_{\odot}$. This model implies 19 ± 3.6 GMCs with masses $M_{\text{GMC}} > 10^6 M_{\odot}$ and orbiting at $R > 8$ kpc, which could interact with the Pal5 stream; 6.9 ± 2.7 of these could interact with GD1 too, since they orbit at $R > 12$ kpc. Mass and radius distributions are generated using different random seeds in different runs, and we explore 15 such initial conditions for each orbit. In each run, GMCs are represented by smoothed massive particles, using the gravitational softening kernel adopted by Gadget2 (Springel 2005). Conservatively, we use a softening length of $\epsilon = 100$ pc, independent of GMC mass, corresponding to the size of the largest Galactic GMCs (e.g., Evans 1999; Lada 2005). We fix the maximum time step to 0.07 Myr, so that, at a relative velocity of 300 km/s, the crossing of a length ϵ is resolved with a minimum of ~ 4.5 steps. GMC lifetimes are much shorter than the dynamical timescales involved here, but we assume the population remains stationary and enforce this by letting our GMCs live through the full duration of each run.

2.1 Example streams

Figure 1 displays a few examples of streams from our suite of simulations of Pal5- and GD1-like orbits (column 1 at $t = 6$ Gyr, and column 2 at $t = 7$ Gyr). All panels show the two-dimensional density distribution of the stream when

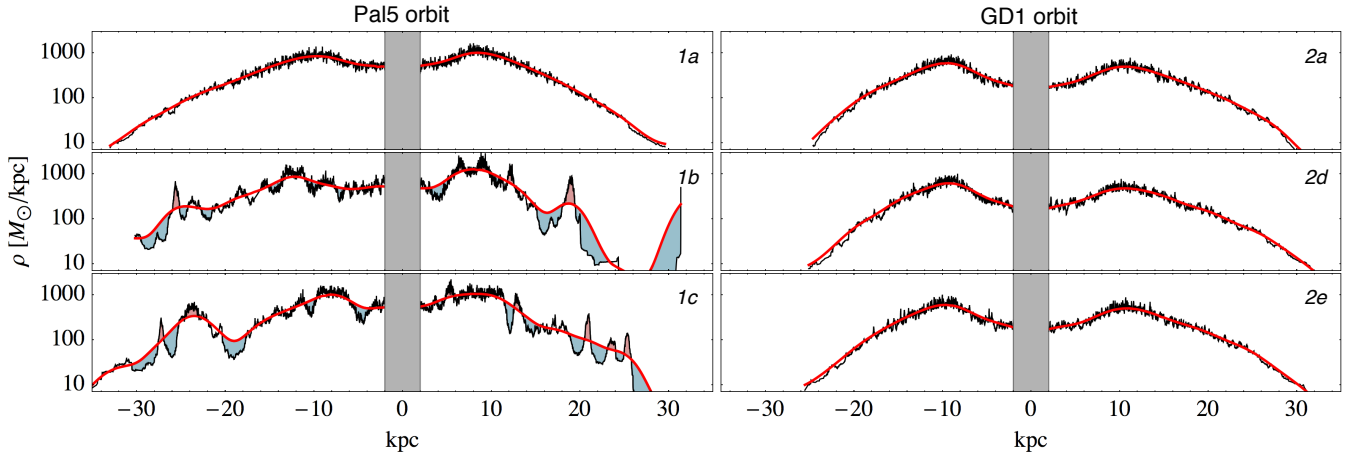


Figure 2. Examples of density gaps and clumps; panels are labelled as in Fig. 1. In all panels, the black profile shows the 1-d density distribution of the stream, while a smoothed profile is shown in red. Shaded gaps and clumps satisfy the selection criteria given in equ. (2).

projected onto the plane perpendicular to the instantaneous orbital angular momentum vector of the remnant cluster. Streams are straightened using a curvilinear coordinate system defined by the GC orbit: the x coordinate denotes distance along the orbit relative to the current position of the remnant, while the y coordinate denotes distance perpendicular to the orbit in projection onto this plane. The remnant itself has been excised from the plots for convenience. The Galactic centre is in the negative y direction, so that the orbital motion in all panels is from left to right.

The top panels, *1a* and *2a*, illustrate runs in which the streams orbit undisturbed within the smooth Galactic potential, resulting in unperturbed density distributions. In both columns the remnant is close to apocenter at the chosen time, so that the ‘feathers’ are particularly evident, in the form of short diagonal over-densities located within a few kpc of the remnant. These are armlets shed during recent pericentre passages. Their shape is a consequence of the orbital properties of the member stars (e.g., Küpper et al. 2012; Mastrobuono-Battisti et al. 2012; Amorisco 2015), and is unrelated to external disturbances. Panels *1b-c* and *2b-c* show examples of prograde streams evolved in the presence of a disk of GMCs, each generated with a different random seed. In all cases, clear disturbances are evident, in the form of gaps and clumps which are visually similar to those generated by flybys of DSs (see for example Fig. 6 of Ngan & Carlberg 2014). Panels *1d-e* and *2d-e* show examples of streams of GCs on retrograde orbits. With respect to the prograde cases, the relative velocities of encounters are increased here, reducing their perturbing effects.

3 RESULTS

Figure 2 shows 1-d density profiles for a selection of the streams displayed in Fig. 1, obtained by collapsing the 2-d distributions along the y direction. In each column, the top panel corresponds to the unperturbed stream, while the lower 2 panels show the prograde cases for Pal5 and the retrograde cases for GD1 (corresponding to the actual observed orbits). The shaded area $|x| \leq 2$ kpc is excised from all the

analyses that follow, so to avoid possible substructure due to the feathers. We isolate any pronounced gaps and clumps and characterise their abundance and properties.

Black density profiles are obtained by using a running bin with adaptive size, containing a fixed number of stream particles, $n = 50$. The bin is moved across the stream one particle at a time. Such profiles are then smoothed with a Gaussian kernel, to obtain the red density profiles, of rms width λ , taken to be a fraction of the total length of unperturbed streams at that time (the values used are collected in Table 1). We define gap (and clump) candidates as all those instances in which the unsmoothed 1-d density profile is continuously below (above) the smoothed profile, and for each we measure the linear size l and relative mass contrast δ , defined as

$$\delta \equiv \begin{cases} M_{\text{sm}}/M & \text{if } M_{\text{sm}} \geq M \\ M/M_{\text{sm}} & \text{if } M_{\text{sm}} < M \end{cases}, \quad (1)$$

where M is the mass in the gap or clump, and M_{sm} is the mass in the same region according to the smoothed density profile. As shown in Fig. 2, density perturbations show a range of sizes and mass contrasts. We concentrate on the strongest perturbations, which are the most interesting for comparison with observation, and which we define as those satisfying the criteria

$$\begin{cases} \delta > 1.4 ; l > 0.4 \text{ kpc} & \text{for gaps,} \\ \delta > 1.4 ; l > 0.2 \text{ kpc} & \text{for clumps.} \end{cases} \quad (2)$$

No such prominent perturbations are found in our undisturbed streams. All gaps and clumps satisfying these criteria are shaded in Fig. 2. No such structure is found in the two GD1 streams shown, which only display minor perturbations.

3.1 Abundances and properties

We count all clumps and all gaps that satisfy the criteria of equ. (2) in our suite of streams. We have carried out 15 different runs for each of our four GC orbits, and we study how the abundance of substructure evolves with time, by

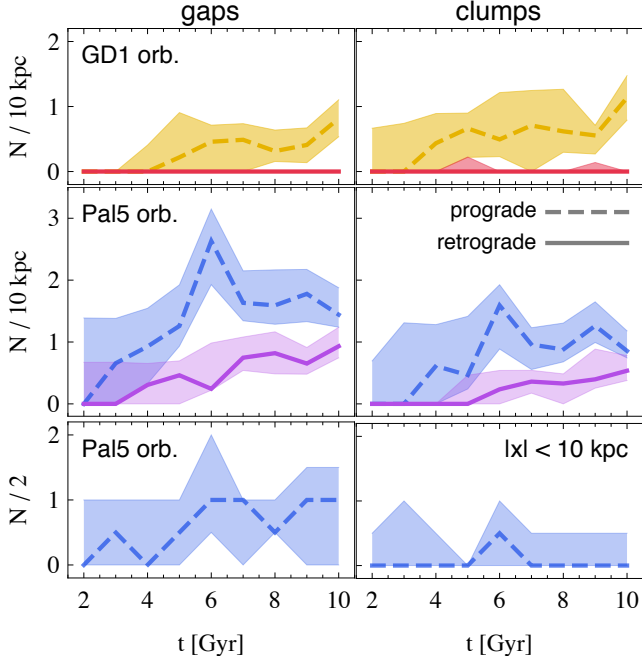


Figure 3. Abundances of gaps (left) and clumps (right) satisfying the criteria of equ. (2). In all panels, lines show the medians, and shaded regions the 10% to 90% range, as a function of stream age. Top and middle panels show distributions of the mean number of perturbations per 10 kpc among the 15 simulations carried out for each GC orbit. N in the bottom panels is the number of perturbations within 10 kpc of the Pal5 remnant, so that $N/2$ estimates the gap (clump) density for the “observed” section of each simulated Pal5 stream.

considering snapshots at intervals of 1 Gyr between 2 and 10 Gyr.

We first measure the average number of gaps (or clumps) in each simulation per 10 kpc of stream length, $\langle N/10 \text{ kpc} \rangle$. We obtain this by dividing the number of perturbations in the stream by its total length, L , defined as the interval in x containing 95% of the stream particles, n_{st} (excluding those in the excised region $|x| \leq 2 \text{ kpc}$; Table 1 lists mean values of L and n_{st} for our streams). Results are displayed in the upper two rows of panels in Fig. 3: the top panels pertain to GD1-like orbits, the middle panels to Pal5-like orbits. Full lines show the medians for retrograde orbits, dashed lines for prograde orbits. Shaded regions span the 10% to 90% range in each set of 15 simulations. A comparison between the top and middle rows shows that GD1 streams form significantly fewer prominent gaps and clumps than Pal5 streams. This is a result of the larger pericentric radius: the Pal5 stream crosses the disk both outside R_{\odot} and within it, where massive GMCs are more abundant. The GD1 stream only experiences encounters with the GMC population at $R \gtrsim 12 \text{ kpc}$, where the latter has a substantially lower density and a steeper mass function. For both Pal5- and GD1-like orbits, the lower encounter velocities of prograde streams result in a systematically higher density of strong perturbations. The density of such perturbations increases weakly with time, as more gaps and clumps grow to exceed the thresholds of equ. (2).

It is not currently known whether a bound remnant of GD1 still exists, nor where it would be located with respect

Table 1. Mean stream length L , mean number of stream particles n_{st} and smoothing length ($\lambda = L_{\text{unp}}/30$, L_{unp} is the length of unperturbed streams) for our prograde Pal5 and retrograde GD1 streams, as a function of time.

t [Gyr]	2	3	4	5	6	7	8	9	10
Pal5									
L [kpc]	18.1	19.5	38.1	45.8	46.6	60.6	66.6	82.2	79.3
$n_{\text{st}}/10^3$	21.2	25.3	31.6	34.5	36.2	41.6	42.3	44.0	47.0
λ [kpc]	0.6	0.6	1.2	1.6	1.6	2.0	2.2	2.6	2.6
GD1									
L [kpc]	19.1	17.7	27.6	49.9	45.9	47.2	70.0	76.7	77.4
$n_{\text{st}}/10^3$	11.4	13.2	15.9	18.0	18.8	19.8	21.3	22.2	22.6
λ [kpc]	0.6	0.6	0.8	1.7	1.6	1.6	2.3	2.5	2.5

to the observed section of the stream. Our average perturbation density can thus, perhaps, be considered representative for this stream. Fig. 3 shows that its retrograde motion and large pericentric radius result in very few perturbations as prominent as required by equ. (2). Recall, however, that our model is conservative in that we ignore the mass-size relation of GMCs (e.g., Evans 1999; Murray 2011), and soften all GMC particles on the same scale, $\epsilon = 100 \text{ pc}$. This results in a uniform half-mass radius of $r_h \approx 120 \text{ pc}$, an overestimate for the bulk of the population. Though rare, this is relevant in those cases in which the point of closest approach during the flyby is smaller than this scale.

On the other hand, the average measurements just presented may overestimate the number of perturbations in the observed section of the Pal5 stream, which only extends about 10 kpc from the remnant. Material in this region has been shed more recently (and so has experienced fewer disk crossings) than material further down the tails. In addition, it is dynamically younger so that any perturbations have had less time to grow above the thresholds of equ. (2)). For our Pal5 prograde streams, we therefore count the number of strong gaps and clumps within 10 kpc of the remnant, N . Results are plotted in the bottom panels of Fig. 3, as $\langle N/2 \rangle$, providing an estimate of the number of perturbations expected within the observed section of the Pal5 stream. The upper panels of Figure 4 illustrate the range of properties of such gaps and clumps, by collecting all of those we identify in the younger section, $|x| < 10 \text{ kpc}$, of our prograde Pal5-like runs. Color coding indicates time and the dashed lines identify the criteria (2). The populations of both gaps and clumps extend to sizes of $\sim 2 \text{ kpc}$ and gaps reach mass contrasts $\delta \gtrsim 2$. The lower panels of the same Figure collect substructure located over the full length of the prograde Pal5 streams. This increases the range of sizes and mass contrasts even further. As ‘older’ gaps and clumps that have streamed far from the remnant are included, a color gradient across the scatter plots becomes apparent, illustrating how the internal dynamics of the stream amplifies perturbations (see e.g., Erkal & Belokurov 2015).

4 DISCUSSION

We have shown that the Galactic population of GMCs can significantly perturb kinematically cold globular cluster streams. Using a flat prior (3 to 10 Gyr) for the age of

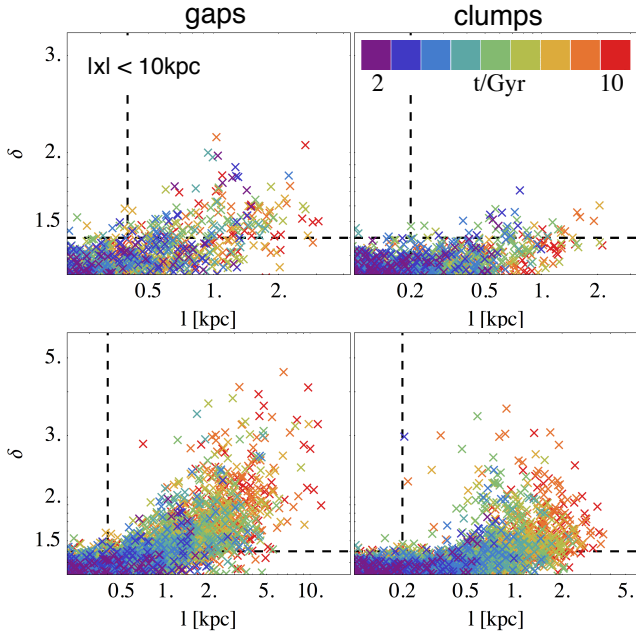


Figure 4. Properties of clumps (right) and gaps (left) in our Pal5-like streams, as a function of stream age (encoded by colour). The top panels show results for the ‘observed’ regions within 10 kpc from the remnant, the lower panels for the streams as a whole.

the Pal5 stream we find that the observed ~ 10 kpc long section of the stream is expected to show $0.5_{-0.5}^{+0.5}$ gaps (median and 10% and 90% quantiles; 0.65 ± 0.5 , mean with one standard deviation) wider than 0.4 kpc and with a mass contrast $\delta > 1.4$. Our GD1 streams, in contrast, experience fewer strong GMC perturbations because of their larger pericentre and the steeper mass function of the GMCs in the outer disk (Heyer & Dame 2015; Rice et al. 2016). Additionally, they are less sensitive to each encounter because of the higher relative velocities resulting from the retrograde orbit. Structures more prominent than the thresholds of equ. (2) are rare in our GD1 streams, at least in our conservative numerical setup, in which all GMCs are smoothed on a scale of $\epsilon = 100$ pc. Weaker but significant gaps and clumps are still present, and may be detectable as enhanced noise in sufficiently deep observations. We defer the quantification of such perturbations to follow-up work.

Currently available observations do not seem to show obvious evidence for prominent gaps (e.g., Ibata et al. 2016; Carlberg 2016; Thomas et al. 2016). However, our results suggest that deep enough observations of the Pal5 stream (and possibly of the GD1 stream) should detect perturbations of GMC origin, even if there is no structure induced by dark matter subhaloes. This re-sets expectations for GC streams in Milky Way models with smooth haloes. Carlberg (2012, 2016) find the Pal5 and GD1 streams to display more substructure than is expected from counting noise alone. From a statistical standpoint, more detailed studies are needed both of observational systematics such as photometric and background-subtraction uncertainties and of theoretical systematics reflecting uncertainties in the stream structure expected in the absence of small-scale perturbations. Only then will it be possible to establish whether apparent inhomogeneities such as those marginally detected in

the Pal5 stream by Bovy et al. (2016) result from encounters with GMCs or with DSs. Distinguishing between these two is made challenging by the absence of clear predictions for the abundance of DM substructure in the haloes of disk galaxies like the MW, where disk shocking and the enhanced tidal field destroy DSs more easily than in DM-only simulations (D’Onghia et al. 2010; Peñarrubia et al. 2010). This is particularly uncertain at the small galactocentric distances of observed GC streams.

In the event of a clear detection of density perturbations of external origin, direct modelling may allow DS and GMC perturbers to be distinguished. Erkal & Belokurov (2015) have shown that by using a combination of both photometric and kinematic data it may be feasible to infer the time since flyby, and the approximate location of the encounter. Given their general framework, the highly constrained spatial and relative velocity distributions of GMC encounters may allow encounters that took place with objects on prograde circular orbits in the disk plane to be distinguished from those that occurred well away from the plane and at very different relative velocities.

ACKNOWLEDGMENTS

NA and SV thank Denis Erkal for stimulating discussions. We thank the referee, Ray Carlberg, for a constructive report.

REFERENCES

- Amorisco, N. C. 2015, *MNRAS*, 450, 575
- Anderson, L., Aubourg, É., Bailey, S., Beutler, F., Bhardwaj, V., Blanton, M., Bolton, A. S., Brinkmann, J. et al. 2014, *MNRAS*, 441, 24
- Bode, P., Ostriker, J. P., & Turok, N. 2001, *ApJ*, 556, 93
- Bovy, J., Erkal, D., & Sanders, J. L. 2016, arXiv:1606.03470
- Bowden, A., Belokurov, V., & Evans, N. W. 2015, *MNRAS*, 449, 1391
- Carlberg, R. G. 2012, *ApJ*, 748, 20
- Carlberg, R. G., Grillmair, C. J., & Hetherington, N. 2012, *ApJ*, 760, 75
- Carlberg, R. G. 2013, *ApJ*, 775, 90
- Carlberg, R. G. 2016, *ApJ*, 820, 45
- Colín, P., Avila-Reese, V., & Valenzuela, O. 2000, *ApJ*, 542, 622
- Diemand, J., Kuhlen, M., Madau, P., et al. 2008, *Nat*, 454, 735
- D’Onghia, E., Springel, V., Hernquist, L., & Keres, D. 2010, *ApJ*, 709, 1138
- Erkal, D., & Belokurov, V. 2015, *MNRAS*, 454, 3542
- Erkal, D., & Belokurov, V. 2015, *MNRAS*, 450, 1136
- Erkal, D., Belokurov, V., Bovy, J., & Sanders, J. L. 2016, arXiv:1606.04946
- Errani, R., Peñarrubia, J., & Tormen, G. 2015, *MNRAS*, 449, L46
- Evans, N. J., II 1999, *ARAA*, 37, 311
- Fritz, T. K., & Kallivayalil, N. 2015, *ApJ*, 811, 123
- Gao, L., White, S. D. M., Jenkins, A., Stoehr, F., & Springel, V. 2004, *MNRAS*, 355, 819

- Gott, III, J. R., Jurić, M., Schlegel, D., Hoyle, F., Vogeley, M., Tegmark, M., Bahcall, N. & Brinkmann, J. 2005, *ApJ*, 624, 463
- Grillmair, C. J., & Dionatos, O. 2006, *ApJL*, 641, L37
- Grillmair, C. J., & Dionatos, O. 2006, *ApJL*, 643, L17
- Heyer, M., & Dame, T. M. 2015, *ARAA*, 53, 583
- Ibata, R. A., Lewis, G. F., Irwin, M. J., & Quinn, T. 2002, *MNRAS*, 332, 915
- Ibata, R. A., Lewis, G. F., & Martin, N. F. 2016, *ApJ*, 819, 1
- Johnston, K. V., Spergel, D. N., & Haydn, C. 2002, *ApJ*, 570, 656
- Klypin, A., Kravtsov, A. V., Valenzuela, O., & Prada, F. 1999, *ApJ*, 522, 82
- Koposov, S. E., Rix, H.-W., & Hogg, D. W. 2010, *ApJ*, 712, 260
- Küpper, A. H. W., Lane, R. R., & Heggie, D. C. 2012, *MNRAS*, 420, 2700
- Küpper, A. H. W., Balbinot, E., Bonaca, A., et al. 2015, *ApJ*, 803, 80
- Lada, C. J. 2005, *Progress of Theoretical Physics Supplement*, 158, 1
- Macciò, A. V., Ruchayskiy, O., Boyarsky, A., & Muñoz-Cuartas, J. C. 2013, *MNRAS*, 428, 882
- Mastrobuono-Battisti, A., Di Matteo, P., Montuori, M., & Haywood, M. 2012, *AA*, 546, L7
- Menci, N., Fiore, F., & Lamastra, A. 2012, *MNRAS*, 421, 2384
- Moore, B., Ghigna, S., Governato, F., et al. 1999, *ApJL*, 524, L19
- Murray, N. 2011, *ApJ*, 729, 133
- Ngan, W. H. W., & Carlberg, R. G. 2014, *ApJ*, 788, 181
- Ngan, W., Carlberg, R. G., Bozek, B., et al. 2016, *ApJ*, 818, 194
- Odenkirchen, M., Grebel, E. K., Dehnen, W., Rix, H.-W., & Cudworth, K. M. 2002, *AJ*, 124, 1497
- Odenkirchen, M., Grebel, E. K., Dehnen, W., et al. 2003, *AJ*, 126, 2385
- Peñarrubia, J., Benson, A. J., Walker, M. G., et al. 2010, *MNRAS*, 406, 1290
- Planck Collaboration, Ade, P. A. R., Aghanim, N., Armitage-Caplan, C., Arnaud, M., Ashdown, M., Atrio-Barandela, F., Aumont, J., Baccigalupi, C., Banday, A. J. et al. 2014, *AA571*, A16
- Rice, T. S., Goodman, A. A., Bergin, E. A., Beaumont, C., & Dame, T. M. 2016, *ApJ*, 822, 52
- Rocha, M., Peter, A. H. G., Bullock, J. S., et al. 2013, *MNRAS*, 430, 81
- Sanders, J. L., Bovy, J., & Erkal, D. 2016, *MNRAS*, 457, 3817
- Springel, V. 2005, *MNRAS*, 364, 1105
- Springel, V., Wang, J., Vogelsberger, M., Ludlow, A., Jenkins, A., Helmi, A., Navarro, J. F., Frenk, C. S., White, S. D. M. 2008, *MNRAS*, 391, 1685
- Thomas, G. F., Ibata, R., Famaey, B., Martin, N. F., & Lewis, G. F. 2016, *arXiv:1605.05520*
- Vogelsberger, M., Zavala, J., & Loeb, A. 2012, *MNRAS*, 423, 3740
- Yoon, J. H., Johnston, K. V., & Hogg, D. W. 2011, *ApJ*, 731, 58
- Willett, B. A., Newberg, H. J., Zhang, H., Yanny, B., & Beers, T. C. 2009, *ApJ*, 697, 207
- Williams, J. P., & McKee, C. F. 1997, *ApJ*, 476, 166